DELPHI Collaboration

DELPHI 2003-023 CONF 642
23 June, 2003

Measurement of b-quark mass effects in the four-jet rate at LEP

P. Bambade
LAL, Orsay
M.J. Costa, J. Fuster and P. Tortosa
IFIC, València

Abstract

The effect of the heavy b-quark mass on the n-jet rates (n=2-5) is studied using LEP data collected by the Delphi experiment at the Z peak in 1994 and 1995. A preliminary measurement of R_4^{bl}, the normalized four-jet rate of b-quarks with respect to light-quarks ($\ell = uds$), using the CAMBRIDGE jet clustering algorithm is presented. Results are compared at hadron level with generators and massive LO calculations. The validity of approximating massive NLO corrections by their corresponding massless ones is investigated with the aim to measure the b-quark mass in four-jet events.

Contributed Paper for EPS 2003 (Aachen) and LP 2003 (FNAL)

1 Introduction

Mass corrections to the $Z \to b\bar{b}$ coupling are of order (m_b^2/M_z^2), which is too small to measure at LEP and SLC. For some inclusive observables, like jet-rates, the effect is enhanced as $(m_b^2/M_Z^2)/y_{cut}$, where $y_{cut} \ll 1$ is the jet resolution parameter [1]. The effect of the b-quark mass in the production of three-jet event topologies at the Z peak has already been measured at LEP and SLC [2, 3, 4, 5]. This study presents the effect of the heavy b-quark mass on the two, four and five-jet rates[1]. The measurements of three-jet rates from [6] are also shown.

The DELPHI data collected during the years 1994 and 1995 at a center-of-mass energy of $\sqrt{s} \approx M_{\mathrm{Z}}$ have been analyzed. The CAMBRIDGE [7] jet reconstruction algorithm has been used as it is expected to give a smaller theoretical uncertainty [8, 9]. The observables studied are:

$$R_n^{b\ell}(y_{cut}) = \frac{[\Gamma_n(y_{cut})/\Gamma_{tot}]^{Z\to b\bar{b}}}{[\Gamma_n(y_{cut})/\Gamma_{tot}]^{Z\to \ell\bar{\ell}}} \qquad (n = 2, 3, 4, 5) \tag{1}$$

where $[\Gamma_n(y_{cut})/\Gamma_{tot}]^{Z\to b\bar{b}}$ and $[\Gamma_n(y_{cut})/\Gamma_{tot}]^{Z\to \ell\bar{\ell}}$ represent the normalized n-jet cross-sections for b- and ℓ=uds-quarks for the value of y_{cut} considered. In this definition, the flavour of the event is given by the pair of quarks coupling to the Z boson.

The three-jet rates in [6] were compared with the predictions from NLO massive matrix elements (ME) [10, 11, 12]. Massive ME calculations are performed in terms of the pole mass M_b or the running mass $m_b(\mu)$. The mass of the b-quark can then be extracted in both definitions from the measured rates. In this note the four-jet results are compared to massive LO ME [13], and the consistency with the three-jet result is tested. Improvements using massless NLO corrections to the four-jet rate [14, 15] were studied. The experimental results are also compared to the PYTHIA 6.131 [16], HERWIG 6.1 [17], and ARIADNE 4.08 [18] event generators.

In this study, the comparison between data and theory (ME or event generators) is done *after* the hadronisation phase. Therefore data results are corrected for detector and kinematical effects, while ME calculations, computed at parton level, are corrected for hadronisation. The parton level is defined as the final state of the parton shower (in PYTHIA and HERWIG) or dipole cascade (in ARIADNE) in the simulation, before hadronisation.

2 Experimental method

2.1 Preselection cuts

Hadronic events are selected in the same way as in [2]:

- Charged and neutral particles are reconstructed as tracks and energy depositions in the detector. A first selection is applied to ensure a reliable determination of their momenta and energies (see Table 1).
- The information from the accepted tracks is combined event by event and hadronic events ($Z \to q\bar{q}$) are selected (see Table 1).

[1] We define R_5^q as $\sum_n R_n^q$ for $n \geq 5$. With this definition all events can be classified belonging to a $n = 2, 3, 4$ or 5-jet topology

- The last step involves a specialised selection for each jet-rate. In order to reduce the impact of particle losses and wrong energy-momentum assignment to jets in the selected hadronic events, further kinematical cuts were applied. Each selected hadronic event was reconstructed with the CAMBRIDGE algorithm and then the corresponding cuts of Table 2 were applied.

Charged Particle Selection	$p \geq 0.1$GeV/c $25^\circ \leq \theta \leq 155^\circ$ $L \geq 50$cm $d \leq 5$cm in $R\phi$plane $d \leq 10$cm in z direction	
Neutral Cluster Selection	$E \geq 0.5$GeV , $40^\circ \leq \theta \leq 140^\circ$ $E \geq 0.5$GeV , $8^\circ(144^\circ) \leq \theta \leq 36^\circ(172^\circ)$ $E \geq 1$GeV , $10^\circ \leq \theta \leq 170^\circ$	HPC FEMC HAC
Event Selection	$N_{ch} \geq 5$ $E_{ch} \geq 15$ GeV $\lvert\sum_i q_i\rvert \leq 6, i = 1, ..., N_{ch}$ No charged particle with $p \geq 40$ GeV/c	

Table 1: Particle and event selection; p is the momentum of particles, θ the angle between the particle and the beam-axis, L the measured track length, d the impact parameter of the track with respect to the interaction point, q_i the charge of the particle, E the energy of associated cluster in the calorimeters, N_{ch} the number of charged particles and E_{ch} the total energy of the charged particles in the event. After applying all these cuts, a sample of 1.15×10^6 hadronic Z decays was selected.

2.2 Overview of the correction method

To measure[2] $\widetilde{R}_2^{\,b\ell}$, we used the method explained in [6]:

$$\widetilde{R}_2^{\,b\ell} = \frac{[c_B^\ell d_{2B}^\ell + \lambda_2 c_B^c d_{2B}^c] - [c_L^\ell d_{2L}^\ell + \lambda_2 c_L^c d_{2L}^c]\widetilde{R}_2^{\,b\ell-det}}{c_L^b d_{2L}^b \widetilde{R}_2^{\,b\ell-det} - c_B^b d_{2B}^b} \qquad d_{2Q}^q(y_{cut}) = \frac{\widetilde{R}_{2Q}^{\,q}(y_{cut})}{\widetilde{R}_2^q(y_{cut})} \quad (2)$$

where the measured rate $\widetilde{R}_2^{\,b\ell-det}$ is corrected using purities ($c_Q^q = N_Q^q/N_Q$) and detector corrections (d_{2Q}^q) taken from the simulation. $Q = B, L$ denotes, respectively, the b and ℓ-tagged samples and q is the true flavour of the sample. The factor $\lambda_2 = \widetilde{R}_2^{\,c\ell}$ is also taken from the simulation: typical values are $\lambda_{2j} = 1.005$ and $\lambda_{3j} = 0.995$. This method has the following advantage: the same procedure to tag flavours, described in the next section, can be used simultaneously in the n-jet sample and in the inclusive sample giving

[2]To simplify notation, in the following we will distinguish the observable $\mathcal{O}$ defined at parton level from the same observable measured at hadron level $\widetilde{\mathcal{O}}$ by means of the tilde.

2-jet kinematical selection	$45^\circ \leq \theta_{thrust} \leq 135^\circ$
3-jet kinematical selection	$45^\circ \leq \theta_{thrust} \leq 135^\circ$ $N_j^{ch} \geq 1\ j = 1,2,3$ $E_j \geq 1$ GeV, $j = 1,2,3$ $25^\circ \leq \theta_j \leq 155^\circ$,$j = 1,2,3$ Plararity cut: $\sum_{ij} \phi_{ij} \geq 359^\circ$, $i < j$, $i,j = 1,2,3$
4,5 -jet kinematical selection	$32^\circ \leq \theta_{thrust} \leq 148^\circ$ $N_j^{ch} \geq 1\ j = 1,2,3,4(5)$ $E_j \geq 1$ GeV, $j = 1,2,3,4(5)$ $25^\circ \leq \theta_j \leq 155^\circ$,$j = 1,2,3,4(5)$

Table 2: The kinematical selection is slightly different for each jet rate. A cut on θ_{thrust} is common in all cases. For n-jet rates with $n > 2$ also a minimum energy of $E_{jet} = 1$GeV is required for each reconstructed jet. θ_j is the angle between each jet and the beam-axis. For the three-jet rates, an additional planarity cut is applied on the sum of all jet pair angles.

the normalisation of the observable (see Eq.1). Systematic uncertainties from the flavour tagging are therefore expected to be reduced as, to first order, only ratios of the flavour efficiencies ϵ_{2Q}^q and ϵ_Q^q appear in the expressions:

$$c_Q^q d_{2Q}^q = \frac{\epsilon_{2Q}^q N^q}{\epsilon_Q^q N^q + \epsilon_Q^{\text{non}-q} N^{\text{non}-q}} \tag{3}$$

The method explained above is however not as good for $\widetilde{R_4}^{b\ell}$ and $\widetilde{R_5}^{b\ell}$ because the four and five-jet samples are topologically very different from the inclusive one used in the normalisation. Here it is important to optimise the flavour tagging for each topology. The following procedure was preferred, expressing the observable $\widetilde{R_n}^{b\ell}$ at hadron level as:

$$\widetilde{R_n}^{b\ell} = \frac{\Gamma_{tot}(Z \to b\bar{b})}{\Gamma_{tot}(Z \to \ell\bar{\ell})} D_n^{b\ell} \frac{N_{nB}}{N_{nL}} = \left(\frac{1 - R_c - R_b}{R_b}\right) D_n^{b\ell} \frac{N_{nB}}{N_{nL}} \tag{4}$$

where $n = 4,5$, N_{nB} and N_{nL} are respectively the total number of n-jet events tagged as b- and ℓ=uds-quarks, R_b and R_c are the partial decay widths of the Z to b and c-quark pairs and $D_n^{b\ell}$ are detector correction factors. This method is linear in $\widetilde{R_{nb}}$, which also has the advantage of leading to smaller statistical uncertainties.

Equation 4 divides the experimental measurement of $\widetilde{R_n}^{b\ell}$ in two parts:

- First, the CAMBRIDGE algorithm is applied on the DELPHI data collected in 1994 and 1995 and for each analysed y_{cut} the four and five-jet samples are constructed. The numbers N_{nB} and N_{nL} ($n = 4,5$) are measured and corrected for detector effects. For $\widetilde{R_5}^{b\ell}$ the flavour tagging was done forcing the event to four-jets.

- Second, the global normalisation factor $\frac{\Gamma_{tot}(Z\to b\bar{b})}{\Gamma_{tot}(Z\to \ell\bar{\ell})}$ is calculated from the latest combination performed for the R_b and R_c values ($R_b = 0.21646 \pm 0.00065$, $R_c =$

0.1719 ± 0.0031) [19]. Taking into account correlations between the two measurements, the following value was found:

$$\left(\frac{1 - R_c - R_b}{R_b}\right) = 2.826 \pm 0.017 \tag{5}$$

With this procedure the flavour-tagging can be used optimally in the context of the four and five-jet topologies while benefiting from the precise R_b and R_c determinations.

2.3 Flavour tag

To identify the flavour of events, two algorithms are available in DELPHI: the lifetime-signed impact parameter of the charged particles [20] and the combined tagging technique [21]. The first method (IP) discriminates the flavour of the event by calculating the probability $P_{E^+}^{jet}$ of having all particles in the jet generated at the interaction point. For the second technique (COMB), a jet estimator X_{jet} is built as an optimal combination of $P_{E^+}^{jet}$ and a set of additional discriminating variables from the jet. Both methods are designed to identify B-hadrons in the final state and are therefore very sensitive not only to the presence of b-quarks directly coupling to the Z boson, but also to secondary production of b and c-quarks from gluons ($g \to b\bar{b}, c\bar{c}$), a process called *gluon splitting*. They can also be used in an anti-tagging mode, to identify Z boson decays to light quarks.

For a given n-jet topology there are different possibilities to construct an estimator for the flavour of the event from the corresponding variables at jet level. The simplest method is to combine the two most b-tagged jets adding their values into a single estimator $X_{ev} = X_1 + X_2$. For two and three-jet topologies this combination has proved to work well[3], but for 4 and 5-jet events it was found that this procedure leads to big systematic uncertainties for both the b and ℓ-tagged samples, because X_{ev} is strongly biased towards misidentifying events with gluon splitting into heavy quarks.

A different combination was tried to identify b-events in four and five-jet events. Firstly, the most energetic jet in each event was identified (E1) and remaining jets were ordered by proximity to E1 (we shall label them as A1, A2 and A3). The closest jet to E1 was discarded making the hypothesis that it was a gluon jet from E1. Finally, a global estimator was constructed as $X_{4j} = X_{E1} + max(X_{A2}, X_{A3})$. To further reduce the misidentification of events containing gluon splitting to heavy quarks, the event was classified as a light event if the most b-tagged jet was not one of the two most energetic jets. With this new definition, the uncertainty due to $g \to b\bar{b}, c\bar{c}$ events was reduced by factors of 2 and 5, respectively.

The X_{4j} distributions obtained in data and Monte Carlo are compared in Figure 1 for the four-jet sample. The stability of the corrected $\widetilde{N_{4b}}$ and $\widetilde{N_{4l}}$ was tested as a function of the purity of the tagging. This is shown in Figure 2 (a) and (c) for the X_{4j} variable. The stability of the X_{ev} variable applied to the four-jets is also shown for comparison. The cuts used to select b and ℓ-quark samples (see Table 2) were chosen to minimize the total uncertainties on the measurements.

In [6] it was shown that a more stable result is found if the b-quark sample is selected with the combined technique and the ℓ-quark one using only $P_{E^+}^{jet}$. The same prescription was then used for $\widetilde{R_2}^{b\ell}$. For $\widetilde{R_4}^{b\ell}$ and $\widetilde{R_5}^{b\ell}$, using the method with Eq. 4 was found to give

[3]The data/MC agreement of X_{ev} can be seen in [6], together with related systematics

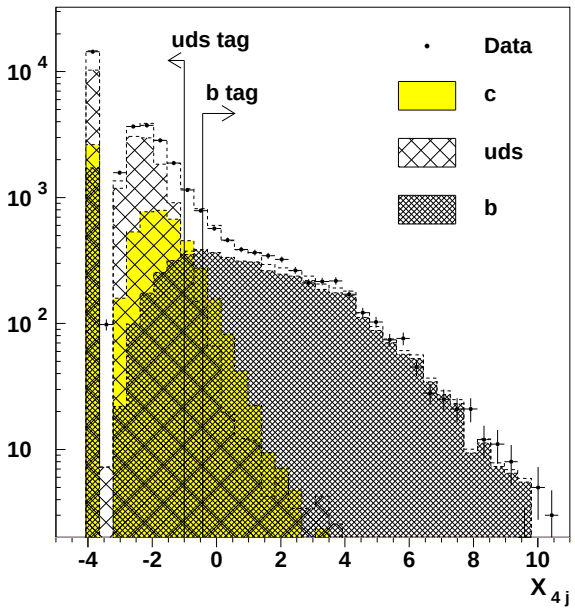

Figure 1: Event distribution of the probability X_{4j} for events classified as four-jets at y_{cut}=0.0085. The real (points) and simulated (histogram) data are compared. The specific contribution of each quark flavour is displayed for the simulated data. The peak at $X_{4j} = -3.8$ marks the events where the most b-tagged jet was not one of the two most energetic jets. The cuts used to tag the b-quark and ℓ-quark samples are also indicated.

stable and compatible results with both techniques. The combined method was chosen because higher purities could be reached with the same efficiency.

2.4 Detector corrections

The detector corrections $D_n^{bl}(y_{cut})$ take into account the flavour identification procedure, kinematic biases, the acceptance and other detector effects. They are calculated with $\sim 4.3 \times 10^6$ hadronic events generated using JETSET 7.3 [22] and treated by the full simulation of the DELPHI detector (DELSIM) and by the standard data reconstruction chain. The simulation was reweighted in order to reproduce the measured gluon splitting rates [23]:

$$\begin{aligned} g_{c\bar{c}} &= 0.0296 \pm 0.0038 \\ g_{b\bar{b}} &= 0.00254 \pm 0.00051 \end{aligned} \qquad (6)$$

3 Comparison with theoretical calculations

3.1 Massive perturbative calculations

For a given flavour q, the n-jet rate is the normalised n-jet cross-section defined as $R_n^q = [\Gamma_n(y_{cut})/\Gamma_{tot}]^{Z\to q\bar{q}}$. Massive ME theoretical calculations exist up to order α_s^2 [10, 11, 12, 13] and describe the 2,3 and 4-jet rates for heavy and light quarks[4]. They have the

[4]In the following, $q(m)$ will stand both for heavy ($q(m) \equiv b(m)$) and light quarks ($q(m) \equiv \ell(0)$)

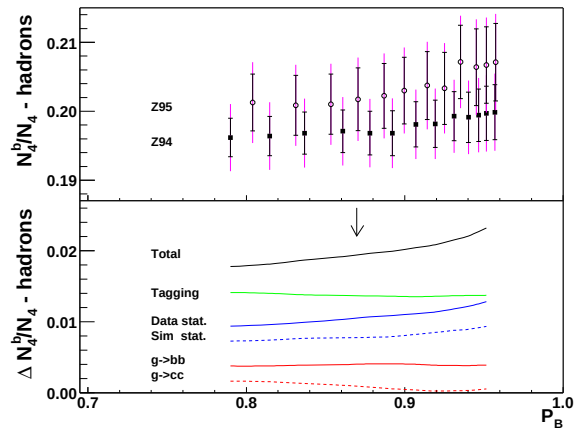

(a) Stability for N_4^b/N_4 with X_{4j}

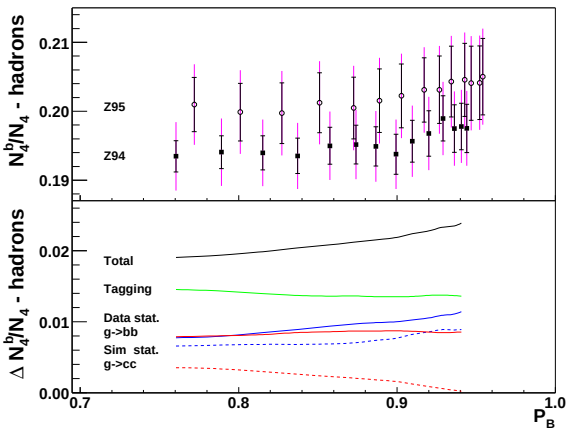

(b) Stability for N_4^b/N_4 with X_{ev}

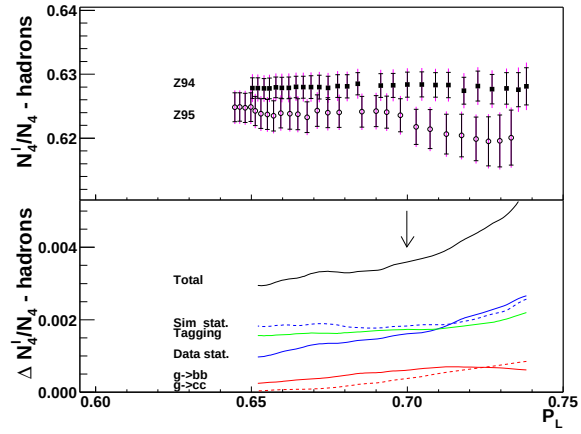

(c) Stability for N_4^ℓ/N_4 with X_{4j}

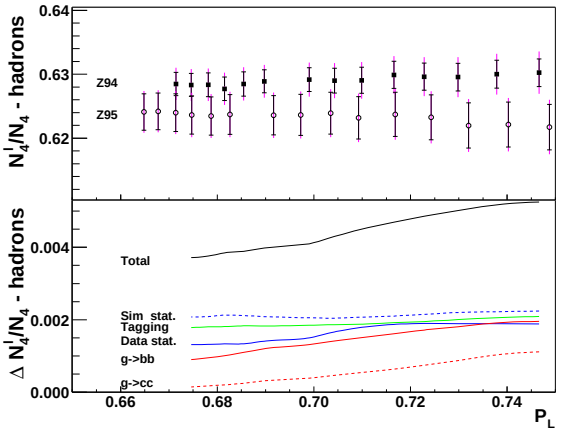

(d) Stability for N_4^ℓ/N_4 with X_{ev}

Figure 2: Stability of the measured four-jet rates as a function of the purity for the two flavour-tagging methods X_{4j} and X_{ev}. The upper part of each plot shows the four-jet rates measured with the 1994 (black squares) and 1995 (empty circles) data. The lower parts show the breakdown of the uncertainties relative to the measured rates. The arrows show the purities resulting from the cuts indicated in Figure 1 for b and ℓ-quark tagging, respectively. The gluon splitting uncertainties from $g_{b\overline{b}}$ and $g_{c\overline{c}}$ are reduced by a factor 2 and 5 respectively if X_{4j} is used.

Method	Type Q	#n-jet events	cut	Purity	Efficiency
Combined	2B	7926	$X_{ev} \geq 0.78$	96%	69%
Impact parameter	2L	109759	$\log P_E^+ > -2.10$	81%	97%
Combined	4B	5195	$X_{4j} \geq -0.43$	87%	48%
Combined	4L	37775	$X_{4j} \geq -1.00$	70%	97%
Combined	5B	251	$X_{4j} \geq -0.43$	79%	34%
Combined	5L	2932	$X_{4j} \geq -1.00$	68%	96%

Table 3: Flavour composition of the 1994 sample ($y_{cut} = 0.0085$) tagged as n-jet b-quark (nB) and ℓ-quark events (nL) for the different jet topologies ($n = 2, 4$ and 5-jets) analysed. The total number of events found in the data samples after cuts was 121302 (2 jets), 44805 (4 jets) and 3304 (5 jets).

structure:

$$\begin{array}{lcllll} R_2^{q(m)} & = & 1 & -(\alpha_s/\pi)A^{q(m)} & -(\alpha_s/\pi)^2(B^{q(m)} + C^{q(m)}) & +\mathcal{O}(\alpha_s^3) \\ R_3^{q(m)} & = & & +(\alpha_s/\pi)A^{q(m)} & +(\alpha_s/\pi)^2 B^{q(m)} & +\mathcal{O}(\alpha_s^3) \\ R_4^{q(m)} & = & & & +(\alpha_s/\pi)^2 C^{q(m)} & +\mathcal{O}(\alpha_s^3) \end{array} \quad (7)$$

To simplify the notation, the dependence on y_{cut} has been omitted in the above expresion. The closure relation $R_2^q + R_3^q + R_4^q = 1$ is satisfied up to order α_s^2. The factors $A^{(m)}$,$B^{(m)}$ and $C^{(m)}$ are computed for massive and light quarks. The calculations are done in the *on-shell* scheme in terms of the pole mass, M_q, and can be rewritten in terms of the running mass, m_q, defined in the $\overline{MS}$ scheme, using the following order α_s relation:

$$M_q^2 = m_q^2(\mu)\left[1 + \frac{\alpha_s(\mu)}{\pi}\left(\frac{8}{3} - 2\log\frac{m_q^2(\mu)}{\mu^2}\right) + \mathcal{O}(\alpha_s^2)\right] \quad (8)$$

It is convenient theoretically to build the double ratios $R_n^{b\ell} = R_n^{b(m)}/R_n^{\ell}$ as this definition cancels most EW corrections, the first order dependence on α_s and partially, the neglected higher order terms. The result is shown in Figure 3 in the case of the $R_4^{b\ell}$ for both mass definitions, at LO and using an approximate NLO prediction (see section 3.2).

3.2 Massless NLO corrections to the four-jet rate

To be able to use Eq. 8 to extract the b-quark mass from the four-jet rate, one would need the NLO correction to R_4^q in (7):

$$R_4^{q(m)} = (\alpha_s/\pi)^2 C^{q(m)} + (\alpha_s/\pi)^3 D^{q(m)} \quad (9)$$

which is available only for massless quarks [14, 15]. However, if most of the mass correction to the observable is already at LO, one may expect to improve the description of the four-jet observable by approximating $D^{b(m)} \approx D^{\ell}$ and therefore correcting both the massive and massless four-jet rates with the massless correction D^{ℓ} [24]. This procedure has been successfully tested for $R_3^{b\ell}$, for which the genuine massive NLO corrections exist. The resulting prediction is shown in Figure 3 [25]. As for the case of $R_3^{b\ell}$ [9], it was found that:

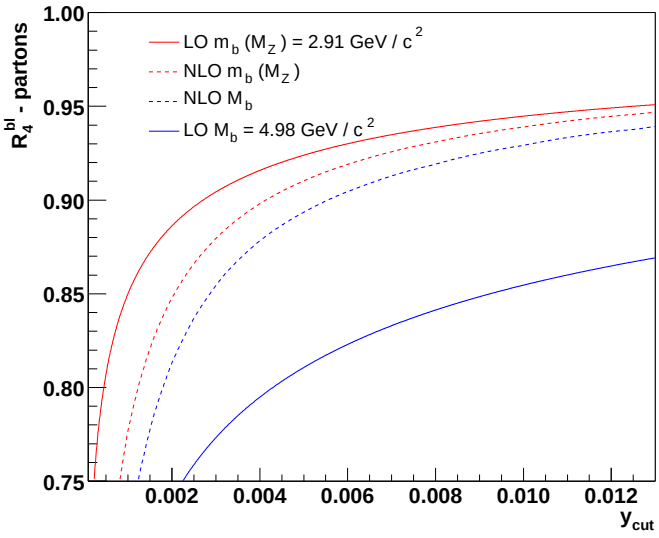

Figure 3: Massive LO ME calculations for $R_4^{b\ell}$(continuous) are shown for both the pole b-mass, M_b, and the running b-mass, $m_b(M_Z)$. Massless NLO corrections are also shown (dashed) as explained in section 3.2 (see equation 9). As for the case of $R_3^{b\ell}$, NLO corrections are smaller for the running mass.

- The NLO corrections using the pole and running mass definitions were both within the uncertainty band defined by the two LO curves.
- The running mass definition gave a smaller correction at NLO than the pole mass.

Such a correction method can be considered plausible for $R_4^{b\ell}$, although one cannot estimate the size of the theoretical uncertainty in a precise way.

3.3 Hadronisation corrections

To compare the parton-level calculations in sections 3.1, 3.2 of $R_n^{b\ell}$ with the experimental results, they must be corrected for hadronisation effects:

$$\widetilde{R_n^{b\ell}} = H_n^{b\ell} R_n^{b\ell} \tag{10}$$

The factors $H_n^{b\ell}(y_{cut}) = H_n^b(y_{cut})/H_n^\ell(y_{cut})$ are computed using PYTHIA 6.131, HERWIG 6.1 and ARIADNE 4.08 tuned to DELPHI data [26] (see Figure 4).

4 Results

The preliminary $\widetilde{R_n^{b\ell}}$ $(n = 2, 3, 4, 5)$ results at hadron level obtained as a function of y_{cut} by combining the 1994 and 1995 data samples are compared to the predictions from PYTHIA 6.131, HERWIG 6.1 and ARIADNE 4.08 generators in Figure 5. None of the three models describe all the measurements perfectly.

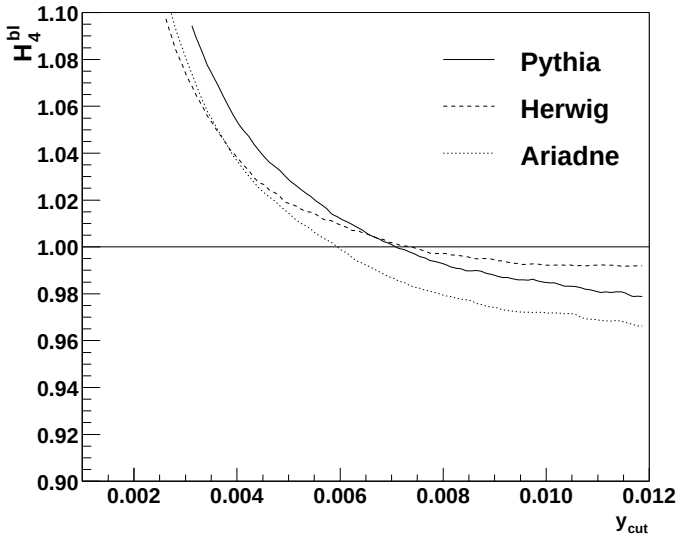

Figure 4: Hadronisation corrections $H_4^{b\ell}(y_{cut}) = \widetilde{R}_4^{\,b\ell}(y_{cut})/R_4^{b\ell}(y_{cut})$ used to correct massive ME four-jet calculations to hadron-level. The correction is below 3% for $y_{cut} > 0.006$.

In the case of the four-jet rates, experimental results were compared to the massive ME calculations at LO and using the massless NLO corrections described in Section 3.2. The results for the four-jet rates for b and ℓ-quarks $\widetilde{R}_4^{\,b}$ and $\widetilde{R}_4^{\,\ell}$ are shown in Figures 6a and 6b for the running mass definition. The massless NLO corrections improve the description of the data in the whole y_{cut} region as much for $\widetilde{R}_4^{\,b}$ as for $\widetilde{R}_4^{\,\ell}$. The upper plot in Figure 6c show the comparison of $\widetilde{R}_4^{\,b\ell}$ with LO ME calculations for the two definitions of the b-quark mass. The lower part shows the effect of the massless NLO corrections described in Section 3.2. A slightly better agreement between data and the QCD prediction was found, particulary for the pole mass definition.

The value of the running mass used in the calculations was taken from the world average in [27], $m_b(m_b) = 4.24 \pm 0.11\,\mathrm{GeV/c^2}$ evolved to $\sqrt{s} = M_Z$ using the QCD renormalisation group equations (RGE). The obtained result was: $m_b(M_Z) = 2.91 \pm 0.10$. For the calculation with the pole mass definition, the determination $M_b = 4.98 \pm 0.13\,\mathrm{GeV/c^2}$ [28] was used.

Comparing the experimental result from $\widetilde{R}_4^{\,b\ell}$ with the ME calculations (LO with or without massless NLO), one can measure both the running and pole masses of the b-quark. The consistency with the three-jet results of [6], $m_b(M_Z) = 2.96 \pm 0.32\,\mathrm{GeV/c^2}$ and $M_b = 4.26 \pm 0.51$, is tested in Figure 7. The results are also compared with the QCD predicted values used for the calculations in Figure 6.

5 Systematic uncertainties

Two different sources of systematic errors have been considered. Experimental uncertainties arise in the process of correcting the detector-level measurement to hadron level. Modelling uncertainties appear in the process of correcting parton-level theoretical

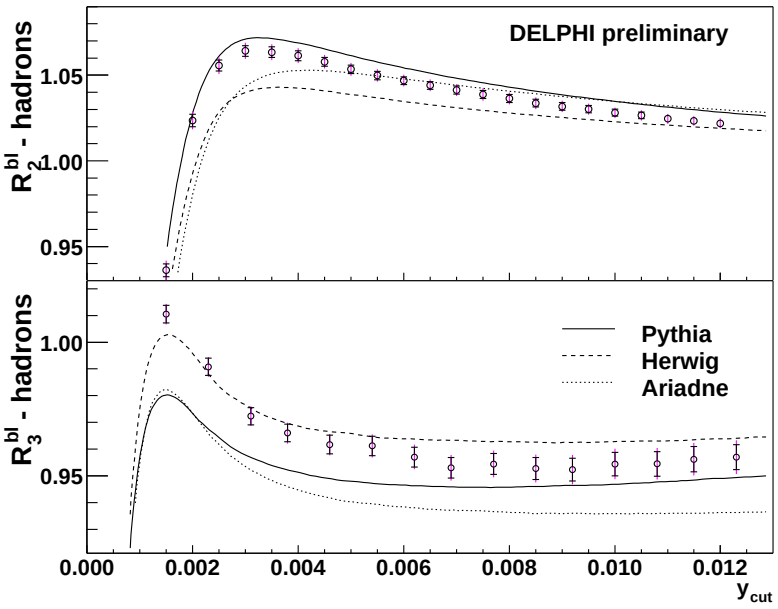

(a) $\widetilde{R_2}^{b\ell}$ and $\widetilde{R_3}^{b\ell}$ compared with generators

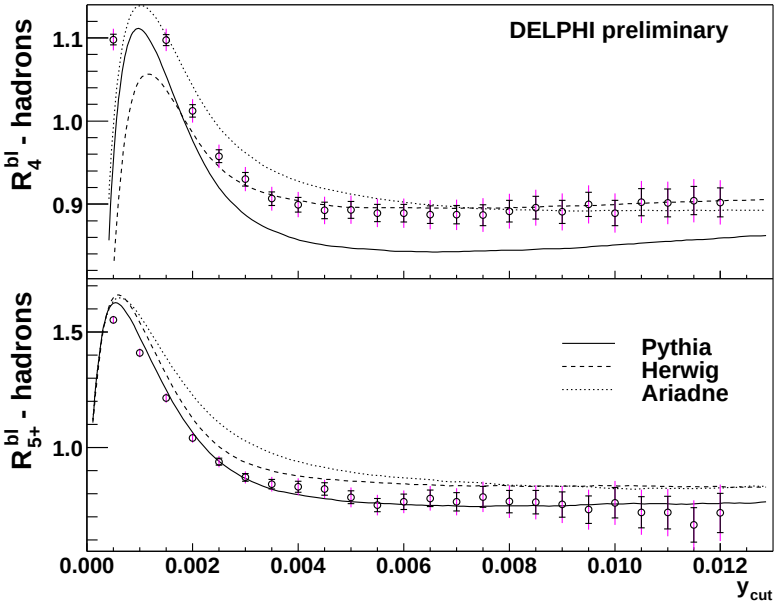

(b) $\widetilde{R_4}^{b\ell}$ and $\widetilde{R_5}^{b\ell}$ compared with generators

Figure 5: Comparison between measured $\widetilde{R_n}^{b\ell}$ rates and predictions from the PYTHIA 6.131, HERWIG 6.1 and ARIADNE 4.08 generators. The data points corresponding to the three-jet rates are from the analysis described in [6].

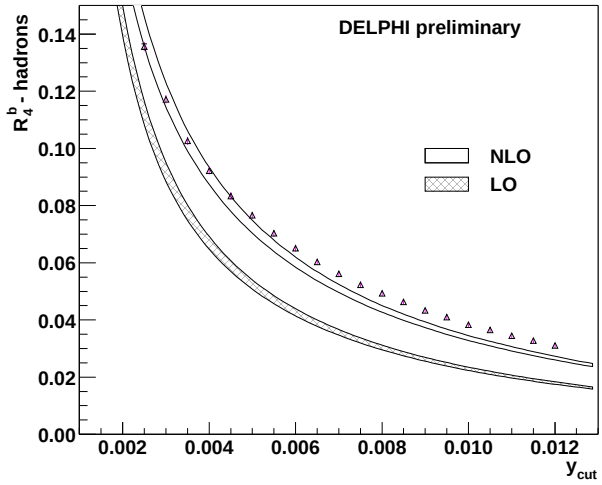

(a) Massive LO with massless NLO in $\widetilde{R}_4^{\,b}$

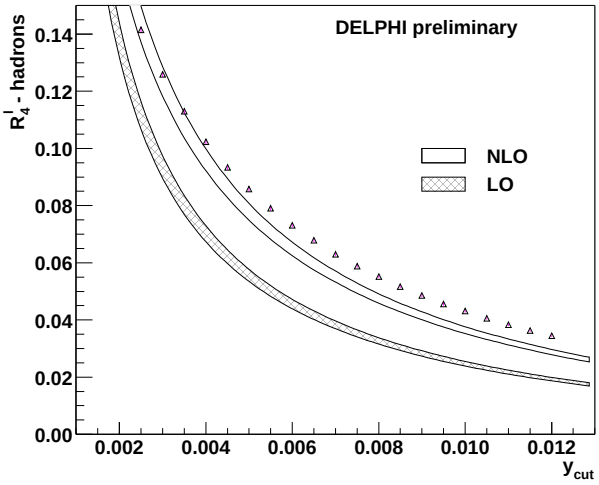

(b) Massive LO with massless NLO in $\widetilde{R}_4^{\,\ell}$

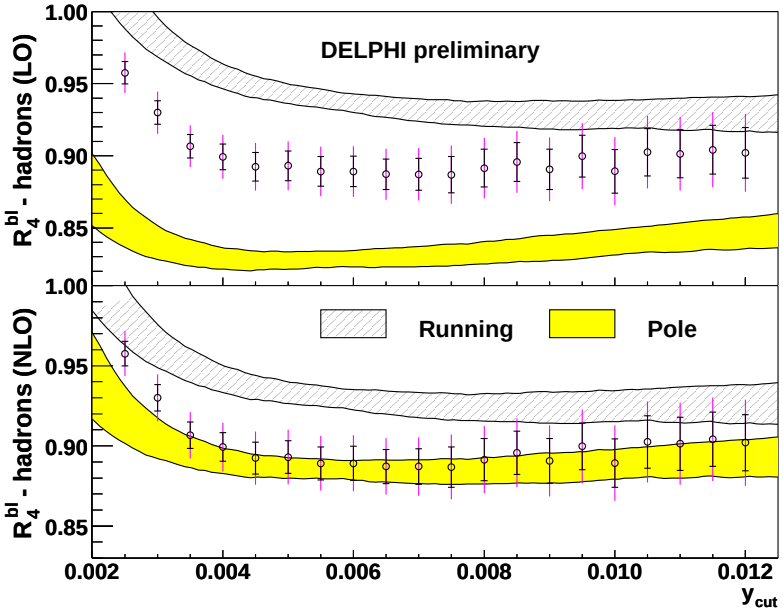

(c) Massive LO with massless NLO in $\widetilde{R}_4^{\,b\ell}$

Figure 6: Comparison between ME predictions corrected for hadronisation and experimental results. The mass values in the calculations were $4.98 \pm 0.13\,\mathrm{GeV/c^2}$ for the pole mass and $m_b(M_Z) = 2.91 \pm 0.10\,\mathrm{GeV/c^2}$ for the running mass (see text). (a) $\widetilde{R}_4^{\,b}$ computed with the running mass definition for massive LO and massless NLO corrections; (b) $\widetilde{R}_4^{\,\ell}$ computed at LO and NLO; (c) Above: massive LO calculations. Below: massive LO predictions with NLO massless corrections. The bands indicate the RMS spread of the three models (see Section 5).

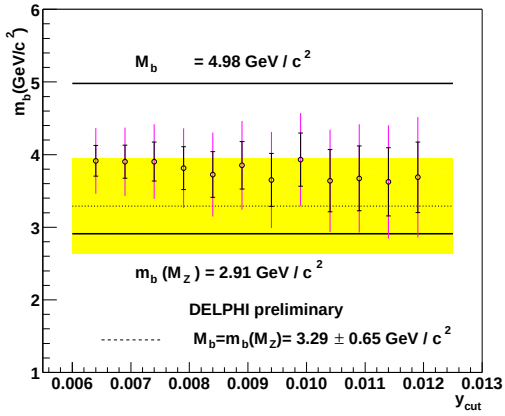

(a) Massive LO

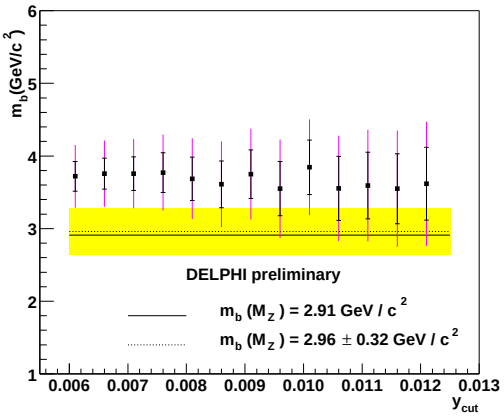

(b) Massless NLO: Running mass

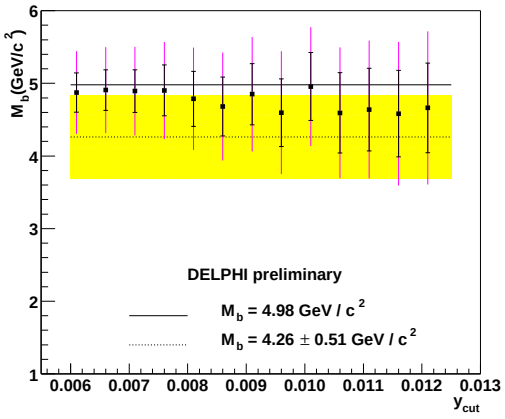

(c) Massless NLO: Pole mass

Figure 7: (a) Massive LO results extracted from $\widetilde{R}_4^{b\ell}$ compared with the result obtained at LO in the $R_3^{b\ell}$ analysis [6]: $M_b = m_b(M_Z) = 3.29 \pm 0.65\,\mathrm{GeV/c^2}$. Results obtained from $\widetilde{R}_4^{b\ell}$ using massless NLO corrections are shown for the running (b) and pole (c) mass definitions and are compared with the results obtained at NLO in the $R_3^{b\ell}$ analysis: $m_b(M_Z) = 2.96 \pm 0.32\,\mathrm{GeV/c^2}$ and $M_b = 4.26 \pm 0.51\,\mathrm{GeV/c^2}$ respectively, shown as $\pm 1\sigma$ band with its central value as a dashed line. Predicted values from the QCD calculations at low energy described in the text are also shown as continuous lines. For the running mass calculation the massless NLO correction is small resulting in very little effect. On the contrary, for the pole mass the NLO correction is about 10% leading to sizeable effects.

calculations to hadron level.

The following sources of experimental uncertainties have been studied:

- Flavour tagging: relative uncertainties of 2% on ϵ^b_{4B} and of 6% on ϵ^ℓ_{4B} and ϵ^c_{4B} were used based on the results in [29]. These numbers are also used as uncertainties for ϵ^q_{4L} taking into account that $\Delta\epsilon^q_{4L}/\epsilon^q_{4L} \approx \Delta\epsilon^q_{4B}/\epsilon^q_{BL}(\epsilon^q_{4B}/\epsilon^q_{4L})$. These uncertainties were propagated to the final result and the observed variation was taken as the flavour tagging uncertainty.

- The error on the global normalisation factor $(1 - R_c - R_b)/R_b$ was determined by varying R_b and R_c within their statistical and systematical uncertainties. The effect on the measured observable was taken as the normalisation uncertainty.

- Gluon splitting: the gluon splitting rates $g_{c\bar{c}}$ and $g_{b\bar{b}}$ were varied in the range of their quoted uncertainties (6). The observed changes in $\widetilde{R_n}^{b\ell}$ were added in quadrature and taken as the gluon splitting uncertainty[5].

As an additional cross-check, the purities of the b- and ℓ-quark tagged samples are varied over a wide range to test the stability of the result (see Figure 8). No important dependence with the purity is found and the chosen working points are well within the stable region.

Three different generators, each tuned independently to the DELPHI data [26], were used in this analysis: PYTHIA (a parton shower model, followed by string fragmentation), HERWIG (a parton shower model, followed by cluster fragmentation) and ARIADNE (a colour dipole cascade model, followed by the same string fragmentation as in PYTHIA). The mean of the three predictions was used to correct the data.

The following sources of modelling uncertainties have been studied:

- The RMS spread between the prediction of the three models was taken as the systematic uncertainty due to the hadronisation model.

- As explained in [30], the kinematical b-quark mass used in PYTHIA 6.131 at parton level can be identified as the pole mass within the uncertainty of the NLO theoretical calculations used to extract $m_b(M_Z)$ from $R_3^{b\ell}$. The M_b parameter in this generator was then set to a recent determination of the pole mass: $4.98 \pm 0.13\,\mathrm{GeV/c^2}$ [28] and the corresponding uncertainty, assumed to be common to the three generators, was propagated to the final result.

The contribution of the different sources of systematic uncertainty to each measurement together with the final combination are listed in Table 4. The two largest uncertainties were from the b-tagging systematics and from the statistical error.

6 Summary

Preliminary measurements of the $\widetilde{R_n}^{b\ell}$ $(n = 2, 5)$ double jet-rate ratios, obtained using the CAMBRIDGE jet clustering algorithm, have been presented at hadron level and compared

[5] Effects on the normalisation factor $(1-R_c-R_b)/R_b$ were taken into account to avoid double counting.

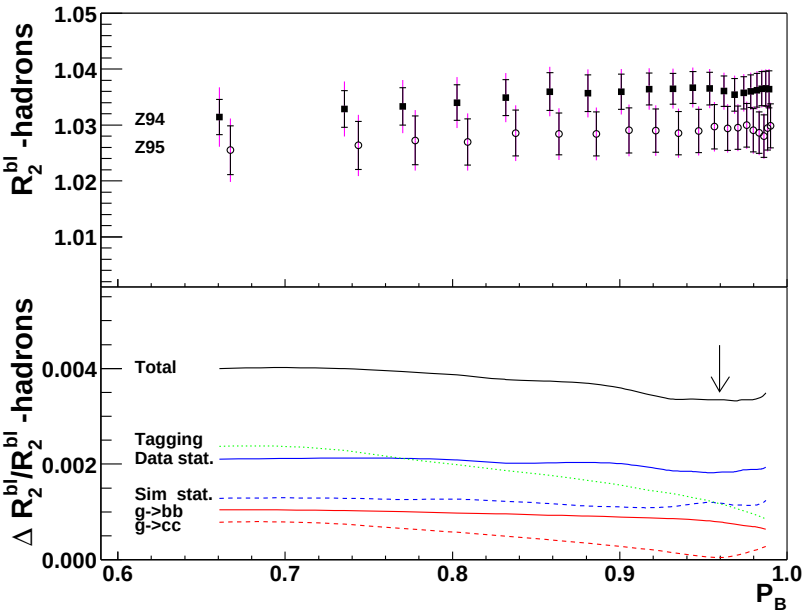

(a)

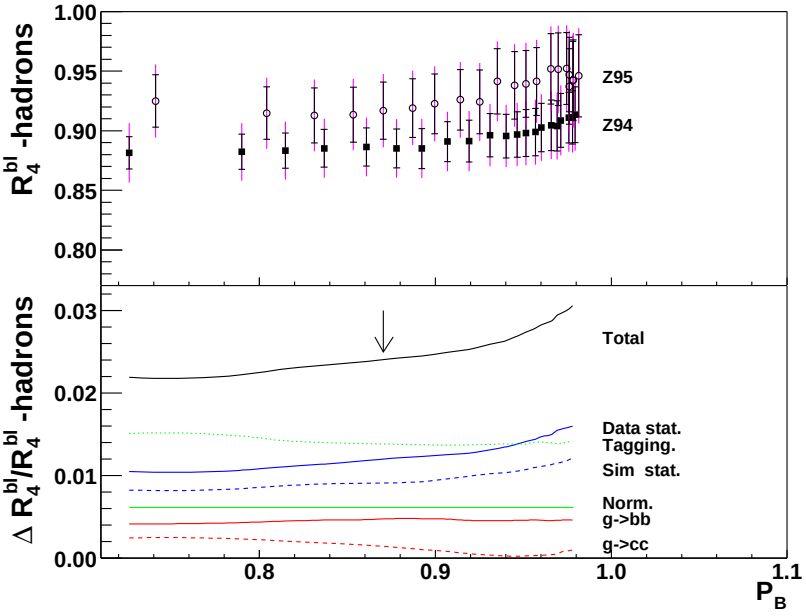

(b)

Figure 8: Stability and systematic breakdown of $\widetilde{R_2}^{b\ell}$ and $\widetilde{R_4}^{b\ell}$ as a function of the purity of the B sample for the chosen working point of y_{cut}=0.0085. The mass effect in the four-observable is twice that of the two-jet observable, while the statistical uncertainty is much higher.

CAMBRIDGE (y_{cut}=0.0085)	$\widetilde{R}_4^{b\ell}$	$m_b(M_Z)\,\mathrm{GeV/c^2}$	$M_b\,\mathrm{GeV/c^2}$
Value	0.898	3.56	4.61
Statistical (data)	$\pm$0.011	$\pm$0.26	$\pm$0.32
Statistical (simulation)	$\pm$0.008	$\pm$0.20	$\pm$0.24
Tagging	$\pm$0.012	$\pm$0.30	$\pm$0.38
Normalization	$\pm$0.006	$\pm$0.13	$\pm$0.16
Gluon splitting:			
($g_{c\bar{c}} = 0.0296 \pm 0.0038$)	$\pm$0.004	$\pm$0.10	$\pm$0.12
($g_{b\bar{b}} = 0.00254 \pm 0.00051$)	$\pm$0.001	$\pm$0.03	$\pm$0.03
Total systematics	$\pm$0.014	$\pm$0.34	$\pm$0.43
Total statistical	$\pm$0.014	$\pm$0.33	$\pm$0.41
Total experimental error	$\pm$0.020	$\pm$0.47	$\pm$0.59
Hadronization	-	$\pm$0.20	$\pm$0.26
Mass parameter	-	$\pm$0.16	$\pm$0.20
Total modelling error	-	$\pm$0.26	$\pm$0.32
Total uncertainty	$\pm$0.020	$\pm$0.54	$\pm$0.67

Table 4: Systematics breakdown for the mass (running and pole) extracted from $\widetilde{R}_4^{b\ell}$ at $y_{cut} = 0.0085$. Experimental and modelling uncertainties (tuning and hadronization) are detailed separately

to the predictions of the PYTHIA, ARIADNE and HERWIG generators (see Figure 5). It was found that none of these generators describe all the measurements perfectly over the full range of y_{cut}.

In the case of the four-jet observable $\widetilde{R}_4^{b\ell}$ a comparison with LO ME calculations, corrected for hadronisation effects based on the mean of the corrections predicted in PYTHIA, ARIADNE and HERWIG, was performed (see the upper plot in Figure 6c). The b-quark mass extracted from this comparison was found to agree well with that extracted from the corresponding three-jet observable [6] using LO expressions (see Figure 7a).

It was also found that the massive LO four-jet rate predictions could be improved using massless NLO corrections (see Figures 6a,b and the lower plot in Figure 6c). The b-quark mass extracted using such approximate NLO predictions was also compared to the three-jet NLO results (see Figures 7b,c). A fair agreement was also found in this last comparison, even though the NLO calculations used are not at the same level of approximation for three and four-jet rates.

7 Acknowledgements

We are grateful to G. Rodrigo and A. Santamaría for providing theoretical input for this measurement. We would also like to thank T. Sjöstrand for his help in understanding how mass effects are implemented in PYTHIA. This work has been partially funded by the IN2P3/CYCIT bilateral funding agreement PP01/1 and the European Research Training Network "The third generation as a probe for new physics", RTN2-2001-00450.

References

[1] G. Rodrigo, M. Bilenky, A. Santamaría, Nucl. Phys. **B439** (1995) 505.

[2] DELPHI Coll., P. Abreu *et al.*, Phys. Lett. **B418** (1998) 430-442;
S. Martí i García, J. Fuster and S. Cabrera, Nucl. Phys. **B** (Proc. Suppl.) **64** (1998) 376.

[3] ALEPH Coll., R. Barate *et al.*, Eur. Phys. J. **C18** (2000) 1.

[4] OPAL Coll., G. Abbiendi *et al.*, Eur. Phys. J. **C21** (2001) 411.

[5] A. Brandenburg, P.N Burrows, D. Muller, N. Oishi, P. Uwer, Phys. Lett. **B468** (1999) 168.

[6] DELPHI Coll., *Determination of the* b*-quark mass at the M_Z scale with the DELPHI detector at LEP*, contribution to this conference, DELPHI-2003-024 CONF 644.

[7] Yu.L. Dokshitzer *et al.*, JHEP **08** (1997) 001.

[8] G. Rodrigo, M.S. Bilenky and A. Santamaría, Nucl. Phys. **B554** (1999) 257.

[9] M. Bilenky, S. Cabrera, J. Fuster, S. Martí i García, G. Rodrigo, A. Santamaría, Phys. Rev. **D60** (1999) 114006.

[10] G. Rodrigo, M. Bilenky, A. Santamaría, Phys. Rev. Lett. **79** (1997) 193.

[11] W. Bernreuther, A. Brandenburg, P. Uwer, Phys. Rev. Lett. **79** (1997) 189.

[12] P. Nason and C. Oleari, Phys. Lett. **B407** (1997) 57.

[13] A. Ballestrero *et al.*, Yellow Report CERN-2000-009 of the LEP2 Monte Carlo Workshop, [hep-ph/0006259].

[14] Z. Nagy and Z. Trocsanyi, Phys. Rev. **D59** (1999) 014020, Erratum-ibid **D62** (2000) 099902.

[15] Z. Nagy and Z. Trocsanyi, Phys. Rev. Lett. **79** (1997) 3604.

[16] T. Sjöstrand *et al.*, Comp. Phys. Comm., **135** (2001) 238;
T. Sjöstrand *et al.*, *PYTHIA 6.2 Physics and Manual*, [hep-ph/0108264].

[17] G. Marchesini *et al.*, Comp. Phys. Comm. **67** (1992) 465;
G. Corcella *et al.*, JHEP **0101** (2001) 010.

[18] L. Lönnblad, Comp. Phys. Comm. **71** (1992) 15.

[19] The LEP Electroweak Working Group and the SLD Heavy Flavour Working Group. LEPEWWG/2002-01.

[20] DELPHI Coll., P. Abreu *et al.*, Z. Phys. **C65** (1995) 555;
G.V. Borisov, C. Mariotti, Nucl. Instr. and Meth. **A372** (1996) 181.

[21] G. Borisov, Nucl. Instr. and Meth. **A417** (1998) 384.

[22] T. Sjöstrand. Computer Physics Commun. **82** (1994) 74.

[23] The LEP/SLD Heavy Flavour Working Group. LEPHF/2001-01.

[24] J. Drees, private communication.

[25] G. Rodrigo, private communication.

[26] DELPHI Coll., P. Abreu *et al.*, Z. Phys. **C73** (1996) 11;
For the tuning of HERWIG 6.1, see M.J. Costa, *Determination of the b quark mass at the M_Z with the DELPHI detector at LEP*, PhD thesis, Universitat de València, 2003.

[27] A.X. El-Khadra and M. Luke, Ann. Rev. Nucl. Part. Sci. **52** (2002) 201.

[28] M. Eidemüller, Phys. Rev. **D67** (2003) 113002.

[29] P. Abreu *et al.*, Eur.Phys.J. **C10** (1999) 415.

[30] P. Bambade, M.J. Costa, J. Fuster and P. Tortosa, *Mass effects in the PYTHIA generator*, DELPHI 2003-061-PHYS-932.